

Solar-Powered Electrochemical Oxidation of Organic Compounds Coupled with the Cathodic Production of Molecular Hydrogen

Hyunwoong Park, Chad D. Vecitis, and Michael R. Hoffmann*

W. M. Keck Laboratories, California Institute of Technology, Pasadena, California 91125

Received: April 1, 2008; Revised Manuscript Received: May 16, 2008

A Bi-doped TiO₂ anode, which is prepared from a mixed metal oxide coating deposited on Ti metal, is shown to be efficient for conventional water splitting. In this hybrid photovoltaic–electrochemical system, a photovoltaic (PV) cell is used to convert solar light to electricity, which is then used to oxidize a series of phenolic compounds at the semiconductor anode to carbon dioxide with the simultaneous production of molecular hydrogen from water/proton reduction at the stainless steel cathode. Degradation of phenol in the presence of a background NaCl electrolyte produces chlorinated phenols as reaction intermediates, which are subsequently oxidized completely to carbon dioxide and low-molecular weight carboxylic acids. The anodic current efficiency for the complete oxidation of phenolic compounds ranges from 3% to 17%, while the cathodic current efficiency and the energy efficiency for hydrogen gas generation range from 68% to 95% and 30% to 70%, respectively.

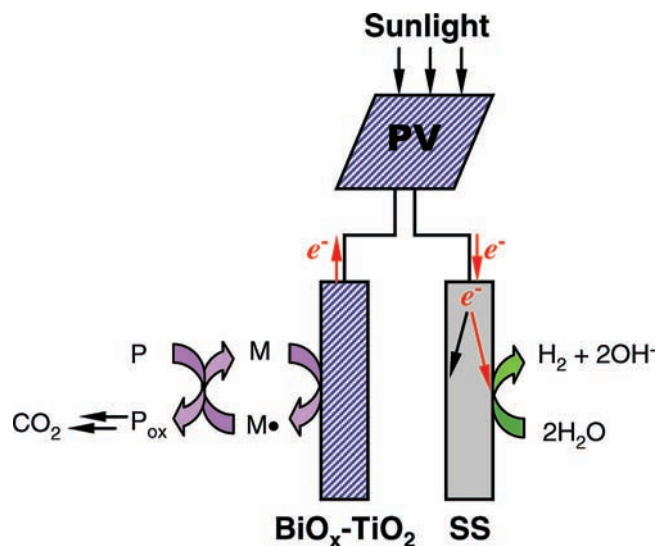
1. Introduction

Hydrogen is under consideration as a viable alternative and renewable energy source in part due to increasing prices of fossil fuels and a growing demand for fuels that are carbon-free and environmentally benign.^{1–3} In the United States alone, the hydrogen market was estimated to have an economic value of \$798 million in 2005; this number is expected to rise to \$1600 million in 2010.³ At the present time, hydrogen is produced primarily by steam-methane reformation (SMR). The SMR accounts for 95% and 48% of all hydrogen produced in the U.S. and in the world, respectively. However, the SMR process has a large carbon footprint in the forms of carbon dioxide and carbon monoxide emissions. For example, the carbon released during SMR is 2.5 times by mass greater than the hydrogen produced.

Electrochemical water splitting (i.e., electrolysis) provides zero-carbon an alternative to the SMR. In this regard, the U.S. Department of Energy (DOE) has established a target energy efficiency of 76% (corresponding to \$2.75/GGE H₂) for hydrogen generation by electrolysis (e.g., by alkaline electrolyzers or proton exchange membrane electrolyzers) by 2015. The current average is 62%.⁴ However, the major component of the cost of electrolytic hydrogen production is not the energy efficiency, but the price of electricity. Therefore, to reduce the overall cost of the electrolysis, low-cost renewable energy sources such as solar light need to be implemented. At the same time, the overall costs could also be reduced by implementation of a dual purpose electrolytic system that couples water or wastewater treatment with hydrogen generation.

The underlying concept of solar-light driven electrolysis integrated with PV system has been previously suggested and tested.^{5–9} The objective is to utilize hydrogen as a storable medium for the dark generation of electricity. This approach is an alternative to a system of PV–electricity–battery. However, the PV–water–electrolyzer systems were found to be economically impractical as compared to the conventional PV–electricity–battery combinations.

SCHEME 1: Schematic Diagram of a PV-Connected Electrochemical Hybrid System for Water Treatment and Hydrogen Production via Water Splitting (Modified from Scheme 1 in Ref 18)



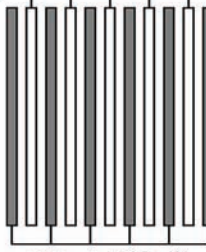
At the same time, the hybrid systems of the electrolytic hydrogen productions and the simultaneous oxidation of organic substrates also have been reported.^{10–12} However, all of the systems operate noncatalytic with much lower efficiency and need severe conditions (e.g., pH < 2, molar ranges of reagents), making them practically nonviable.

Therefore, to address the goal of PV-combined electrolytic hydrogen production and simultaneous oxidation of wastewater constituents, we have combined an electrochemical system advanced oxidation for the treatment of water and wastewater and the electrolytic production of hydrogen. It was found that this hybrid operates not only catalytically but also in mild conditions with relatively high efficiency. More specifically, the anode generates oxidizing radical species (e.g., OH•, Cl•) (R1), which subsequently react with aqueous pollutants while the

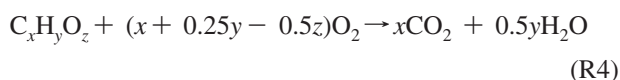
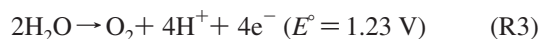
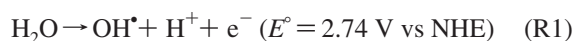
* Corresponding author. Phone: (626) 395-4391. Fax: (626) 395-2940. E-mail: mrh@caltech.edu.

SCHEME 2: (a) General Composition and Preparation Procedure of BiO_x-TiO₂/Ti Anode; (b) Bundle of BiO_x-TiO₂ Anode and Stainless Steel (SS) Cathode Couples for a Subpilot Scaled Electrolysis (20 L)

(a) Over-coat (TiO₂/Bi₂O₃)	TiO ₂ /Bi ₂ O ₃ (Ti:Bi = 90:10 by mol%), 2×(OC, ad, 5@250, H ₂ O, 5@250) 2×(OC, ad, 5@425, H ₂ O, 5@425)
Slurry coat	Bi-doped TiO ₂ (Ti:Bi = 96:4 by mol%), 7×(slurry, OC, ad, 5@250)
Seal coat	SnO ₂ /Bi ₂ O ₃ (Sn:Bi = 90:10 by mol%), 2×(2×(SC), 10min@425)
Precoat (Anti-passivation layer)	IrO ₂ /Ta ₂ O ₅ (Ir:Ta = 67:33 by mol%), 1×(1 hr@525), 5×(10 min@525)
Substrate	Ti-Gr.2 sheet 0.020 inch thick, 2.25×5.75 inches

(b) Anode (0.8 m²)	
Cathode (0.96 m²)	

cathode splits water into hydrogen (R2). Oxygen evolution via water oxidation (R3) is normally the complementary reaction to H₂ production (R2), and thus the generation of radical species (R1) at the anode results in nonstoichiometric water splitting (i.e., H₂/O₂ > 2).



In the past, we developed a Nb⁴⁺-doped polycrystalline TiO₂ anode, which generated hydroxyl radical via one-electron oxidation of water at average current efficiencies at 50%.^{13–16} However, a newer, more robust, and longer lived semiconductor anode based on a mixed metal oxide of BiO_x-TiO₂ has been developed. The Nb⁴⁺-doped electrodes were observed for their lifetime to be significantly shortened at higher current densities, while this BiO_x-TiO₂ electrode is not affected by the magnitude of the current densities for its lifetime. In addition, the BiO_x-TiO₂ electrode operates normally at pH 2–12 without any sign of deactivation. This anode operates at current efficiencies that are in the range of 20–30%.¹⁷ In this study, a BiO_x-TiO₂ anode is coupled with stainless steel cathode and powered by a photovoltaic (PV) array to oxidize organic substrates and to simultaneously generate molecular hydrogen (Scheme 1).^{18,19} Phenol is used as a model chemical substrate because phenolic compounds are a high frequency contaminant present in water and wastewater systems.^{20,21}

2. Experimental Section

2.1. Electrodes. The anode was prepared as follows: (1) A Ti metal sheet (Ti-Gr.2 sheet, 0.50 mm thick) was cleaned using SiC paper (120–240 grit) before coating with a sequence of substrates (Scheme 2a). (2) An initial surface coating containing Ir and Ta at an Ir:Ta = mole ratio of 0.67:0.33 was deposited and annealed to the Ti base. (3) The initial metal oxide coating was sealed with SnO₂ doped with Bi at a Sn:Bi mole ratio of 0.9:0.1. (4) A tertiary surface coating of TiO₂ that was doped with Bi at a Ti:Bi mole ratio of 0.96:0.04 was layered down next with high temperature annealing. (5) The final step involves the deposition of an overcoat that contains a mixture of oxides of Ti and Bi at a Ti:Bi mole ratio of 0.9:0.1. Each successive step of coating requires a specific heat treatment regime at different temperatures and durations. More details are provided elsewhere.¹⁷ Two types of anode–cathode couples were used for the experiments reported herein. The first couple is composed

of a single anode with an active area of contact with the electrolyte solution of 10.0 × 2.0 cm² and two pieces of stainless steel (SS) cathodes (Hastelloy C-22) of the same size facing both sides (i.e., a sandwich configuration) of the doubly coated anode plate with a distance of separation of 2 mm. The second configuration involves a small pilot scale reactor consisting of 5 anode plates (5 pieces × 800 cm²/piece) and 6 stainless steel cathode plates that face each other with a distance of separation of 2 mm (Scheme 2b).

2.2. Electrolysis Experiments. The BiO_x-TiO₂ anode and SS cathode couple was immersed in the electrolyte of 50 mM NaCl (200 mL or 20 L), and the electrolyte was stirred under the continuous purging with air or nitrogen as a background carrier gas. The target substrates (e.g., phenol) were mixed with a background electrolyte or added during the course of electrolysis. A constant cell voltage or current was applied to the electrodes with a DC power supply (HP 6263B and 6260B). For the PV-powered electrolyses, a commercial thin film, amorphous silicon PV (Silicon Solar Inc.), with a peak power output of 6.4 W_{peak} (PV_{peak} = E_{peak} × I_{peak}; E_{peak} = 8–10 V; I_{peak} = 0.95 A) and with active surface area of 1280 cm² was used (Scheme 1). Real-time solar radiation was monitored and recorded with a pyranometer (Apogee) connected to a datalogger (Campbell Scientific). Cell voltage (E_{cell}) and cell current (I_{cell}) were measured by multimeters (Fluke). The current efficiencies (CEs) and the energy efficiencies (EEs) for hydrogen production (i.e., higher heating value) were obtained by the following:

$$\text{CE (\%)} = \frac{\text{number of molecules produced (H}_2, \text{O}_2, \text{ or CO}_2\text{) or degraded (phenol)}}{\text{number of electrons flowed}} \times n \times 100$$

where $n = 2$ and 4 for hydrogen and oxygen production in cathodic current efficiencies (CCEs), respectively. The anodic current efficiencies (ACEs) are described as ACE-I, where $n = 1$ for a one-electron oxidation of phenol, and ACE-II, where $n = 14/3$ for the complete oxidation of a phenolic carbon to CO₂, where the nominal valence state of a carbon in phenol is $-2/3$ while the carbon in CO₂ is in the $+4$ valence state (i.e., a total loss of $+14/3$ electrons per carbon for complete oxidation to CO₂).

DC or PV powered electrolytic H₂ EE =

$$\left(\frac{(39 \text{ W} \cdot \text{h/g} \times \text{H}_2 \text{ rate} \times 2 \text{ g/mol})}{E_{\text{cell}} \times I_{\text{cell}}} \right) \times 100\%$$

$$\text{PV}_{\text{cell}} = E_{\text{cell}} \times I_{\text{cell}} \text{ (applied to the cell reactor)}$$

Solar-to-PV_{cell} EE =

$$\left(\frac{\text{PV}_{\text{cell}} \text{ (W)}}{\text{solar flux (W cm}^{-2}) \times \text{PV area (cm}^2)} \right) \times 100\%$$

Solar-to-H₂ EE =

$$(\text{electrolytic H}_2 \text{ EE} \times \text{solar to PV EE}) \times 100\%$$

2.3. Analytical Procedures. The reactor was sealed from the ambient atmosphere. At a given rate, the headspace gas of the reactor was extracted with a peristaltic pump and pushed through a membrane inlet into a quadrupole mass spectrometry (Balzers) via a turbo pump (Pfeiffer; 5.0×10^{-6} Torr). The volume percent of the headspace was calculated assuming that it was directly proportional to the ion current measured by the mass spectrometer and that the transfer of all gases through the membrane and their 70 eV electron ionization cross-sections were approximately equivalent. This assumption was validated in part because ambient air was measured to be 77% nitrogen, 17% oxygen, 5% water vapor, and 1% argon.

Aqueous organic compounds including intermediates were analyzed by a high performance liquid chromatography (HPLC, Agilent 1100 series) with a C18 column. The eluent was composed of 55% Milli-Q water (0.1 wt % acetic acid) and 45% acetonitrile at flow rate of 0.7 mL/min. Total organic carbon was determined (TOC, OI Analytical Aurora model 1030) with an autosampler (OI Analytical model 1096).

3. Results and Discussion

3.1. Electrolytic Nonstoichiometric Water Splitting. Figure 1 shows a typical DC-powered electrolysis at the BiO_x-TiO₂

anode coupled to the stainless steel cathode couple in the presence of sodium chloride as a supporting electrolyte. Water splitting is initiated at 2.0 V, which is approximately 0.8 V higher than the ideal potential ($E^\circ = 1.23$ V). The rates of H₂ production and O₂ production increase with increasing cell voltage (E_{cell}). Furthermore, cell currents (I_{cell}) also increase in a linear fashion with increasing E_{cell} above 2.1 V. The rates of formation of H₂ and O₂, respectively, are $9.0 \mu\text{mol/min per mA/cm}^2$ and $1.3 \mu\text{mol/min per mA/cm}^2$, which correspond to a nonstoichiometric H₂ to O₂ ratio between 6 and 7 depending on the specific experimental conditions. This indicates some additional anodic reactions (R1) as well as water oxidation (R3) take place simultaneously at the anode. The water oxidation at the surface of a semiconducting metal oxide (MO) anode like TiO₂ is known to proceed by coupling of two surface-bound hydroxyl radicals (R5 and R6):



The current efficiencies for the hydrogen production at the SS cathode are close to 70%, while those for the oxygen production at the BiO_x-TiO₂ anode are in the range of 10–25% (Figure 1c). Despite an initial N₂ atmosphere, H₂O₂ can be produced via superoxide/hydroperoxyl radical pathway at the cathode (R7–R9) due to anodic water oxidation.

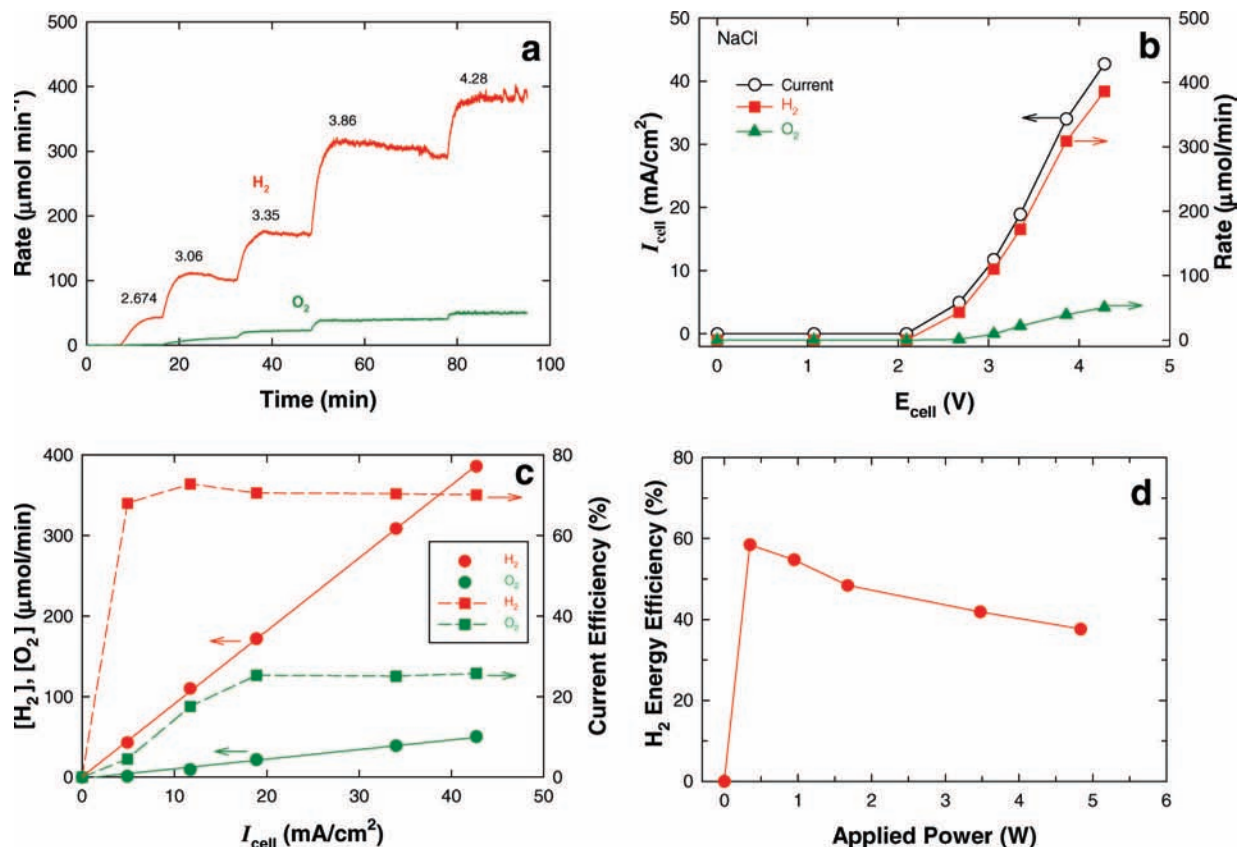
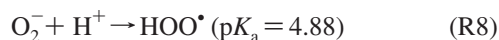


Figure 1. (a) Time profiles of a DC-powered hydrogen and oxygen production rate as a function of cell voltage (E_{cell}) at BiO_x-TiO₂ anode and stainless steel (SS) cathode in 50 mM NaCl solution. (b) Effects of E_{cell} on cell currents (I_{cell}) and the rates of hydrogen and oxygen production. (c) The rates and current efficiencies of hydrogen production and oxygen production as a function of I_{cell} . (d) Effects of applied power on energy efficiencies for hydrogen production. (a) and (b) are taken from ref 18.



The cathodic reaction of R7 will limit the current efficiency for the hydrogen production. The energy efficiencies, which are expressed in terms of higher heating values (HHV) for H₂ production, are in the range of 35–60% (Figure 1d). This value decreases with increasing applied power. However, the energy efficiency can be improved either by reducing an ohmic potential drop in the cell by increasing electrolyte concentration or by coating noble metal (e.g., Pt) on the stainless steel cathode.

3.2. Electrochemical Oxidation of Organic Compounds.

The electrochemical oxidation and complete degradation of phenol at current density of $I = 14 \text{ mA/cm}^2$ is shown in Figure 2. Phenol is completely degraded via first-order kinetics with an apparent half-life of $t_{1/2} = 4.25 \text{ min}$. The end-product of phenol oxidation, CO₂, is detected after 38 min (Figure 2a).

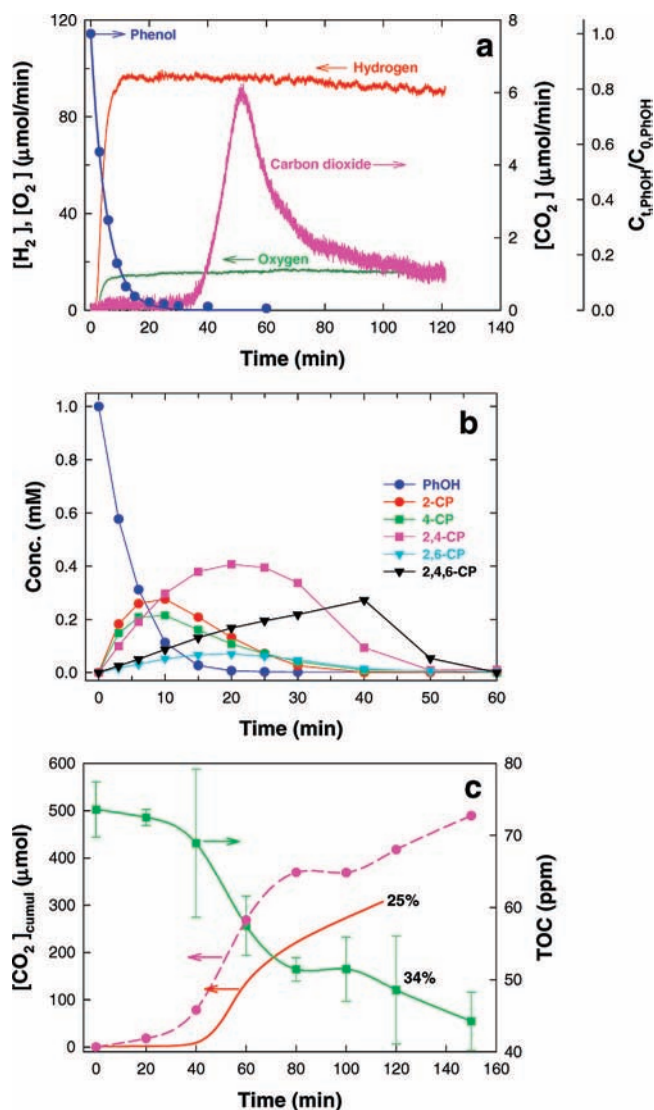
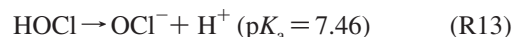
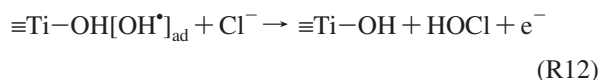
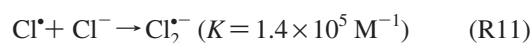
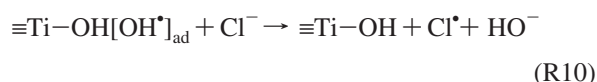


Figure 2. (a) Electrochemical oxidation of phenol to carbon dioxide and simultaneous generation of hydrogen and oxygen at $I_{\text{cell}} = 14 \text{ mA/cm}^2$. (b) Time profiles of intermediates generated during the oxidation of phenol. (c) Time profiles of accumulation of carbon dioxide and TOC decrease. $[\text{phenol}]_0 = 1 \text{ mM}$ (0.2 L); $[\text{NaCl}] = 50 \text{ mM}$; nitrogen purged continuously; Cumulative $[\text{CO}_2]$ was estimated based on TOC decrease.

Under these conditions, the H₂ production rate (i.e., 95 μmol/min) is reduced slightly to 90 μmol/min after the initiation of CO₂ production, while the O₂ production rate is almost unchanged at 15 μmol/min . As the phenol undergoes degradation, mono-, di-, and trichlorinated phenols are formed as intermediates by stepwise chlorination of the parent phenol; however, they are also completely destroyed within 1 h (Figure 2b and Scheme 3). When added separately, the chlorinated phenols also are destroyed as rapidly as phenol with the following order of electrochemical reactivity: 2,4,6-trichlorophenol (3.74) > 2,6-dichlorophenol (1.84) > 2,4-dichlorophenol (1.38) > phenol (1.0) > 2-chlorophenol (0.78) > 4-chlorophenol (0.57). The numbers in parentheses are observed reaction rates relative to phenol. At around 40 min of electrolysis, trichlorophenol begins to degrade rapidly (Figure 2b), and at the same time carbon dioxide is released (Figure 2a). This reduces the total organic carbon (TOC) concentration to decrease dramatically (Figure 2c). It is notable that after 2 h of electrolysis the total amount of CO₂ released accounts for 25% of the initial amount of carbon present in phenol, while CO₂ removal based on the TOC measurements is close to 34%. The “apparent carbon deficit” (~9%) consists of dissolved carbonate (CO₃²⁻) and bicarbonate (HCO₃⁻), which will vary as a function of pH.

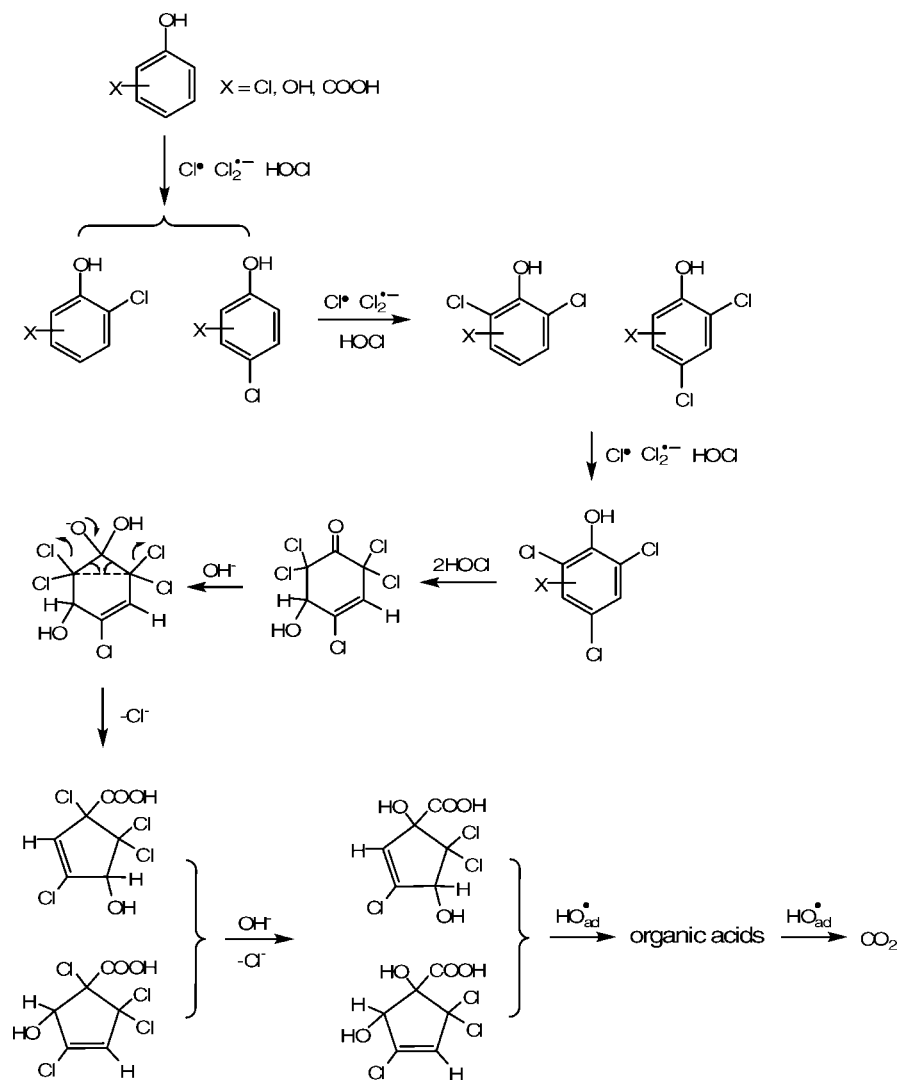
The specific intermediates, which are observed during the electrolytic degradation of phenol, vary depending on the composition of anode surface and on the nature of the supporting electrolyte. In the case of Na₂SO₄, oxygenated or hydroxylated phenols such as catechol, hydroquinone, and benzoquinone are typically found as primary aromatic intermediates.^{22–26} On the other hand, for NaCl, a carbon anode produces the chlorinated phenols while they were not produced at SnO₂/Ti and IrO₂/Ti anodes.²⁷ The electrolysis with NaCl as a background electrolyte is reported to generate active chlorine species such as chlorine radical (Cl[•]), dichloride radical anion (Cl₂^{•-}), and hypochlorous acid/hyperchlorite (HOCl/OCl⁻) via surface-bound hydroxyl radical-mediated pathways (R10–R13):



The rate constants for the reaction of hydroxyl radical, chlorine radical, dichloride radical anion, and HClO with phenol are 6.6×10^9 ,²⁸ 2.5×10^{10} , 2.5×10^8 , and $2.2 \times 10^4 \text{ M}^{-1} \text{ s}^{-1}$,^{29,30} respectively. As a consequence, phenol and its reaction intermediates have at least five different degradation pathways that are mediated by surface-bound/free hydroxyl radicals, chlorine radicals, dichloride radical anions, hyperchlorite ions, and minor hydrogen peroxide (R9).

As the current density is increased, the half-life ($t_{1/2}$) for phenol oxidation along with the anodic current efficiency (ACE-II) for complete oxidation of phenol carbon (charge $-2/3$) to carbon dioxide (charge $+4$) decreases (Figure 3). At the same time, the phase-delayed release of CO₂ decreases from 60, 35, and 22, to 15 min. However, the amount of carbon dioxide released during the course of the electrolysis and the anodic current efficiency (ACE-I) for one-electron oxidation of phenol (PhOH \rightarrow PhOH^{•+} + e⁻) is not altered significantly (Figure 3c). In addition, cathodic current efficiency (CCE) for hydrogen

SCHEME 3: Proposed Reaction Pathway for Electrochemical Degradation of Phenol



production is almost invariable in the range of 50–70%. On the other hand, the initial concentration of phenol markedly affects the apparent degradation rate. The half-life grows linearly with concentration over the range of 0.5–2.0 mM (Figure 4) and increases by 2 orders of magnitude at higher concentrations (i.e., $t_{1/2} = 1.28$ min at 0.5 mM and $t_{1/2} = 150$ min at 10 mM). As the concentration of phenol is increased, a greater number of reaction intermediates are produced, which in turn compete with phenol at the anode surface. This should result in both a decrease in $t_{1/2}$ and a lengthening of the onset time of carbon dioxide release. The anodic current efficiency (ACE-I) is lowered somewhat to 8% at concentrations above 1.0 mM, while the ACE-II ranges from 5% to 10%. On the other hand, CCE is invariable (~68%) to increasing the initial phenol concentration. This indicates that anodic radical production and subsequent organic oxidation does not have a negative effect on the hydrogen production as long as substrates are initially present in the medium; rather, it was observed the anodic treatment of aqueous pollutants enhances the H_2 production rate with a synergistic effect.^{18,19}

We also compared the pure electrolytic efficiency with Na_2SO_4 and NaCl and observed that the degradation rate of phenol in the NaCl is 2 orders of magnitude faster than that in the Na_2SO_4 (Figure 5). Sodium phosphate and carbonate have effects similar to those of sodium sulfate as background

electrolytes. On the other hand, the cathodic H_2 production efficiency in the Na_2SO_4 is higher than that in the NaCl by 23%. When 50 mM NaCl is added to a 50 mM Na_2SO_4 solution at increasing concentrations, the efficiency of phenol degradation increases linearly, but the efficiency of the H_2 production decreases slightly (i.e., CCE at 50 mM $\text{Na}_2\text{SO}_4 = 95\%$; CCE at 50 mM $\text{Na}_2\text{SO}_4 + 50$ mM $\text{NaCl} = 73\%$; CCE at 50 mM $\text{NaCl} = 68\%$). This indicates the anode is active primarily for the generation of oxidative chlorine radical species.

During the course of electrolysis of water and electrolyte alone, the pH of solution rises initially from pH 6 to 10 and then remains constant throughout. After the electrolysis is stopped, it falls to 9.5 (Figure 6). In contrast, when electrolysis takes place in the presence of phenol, the pH increases to initially to 11 and then decreases quickly to 7 after 10 min and then remains in the circum-neutral range (pH ~7.5) during the latter stages of electrolysis. The cathodic reduction of protons results in a rise in the measured pH. However, the progressive oxidation of phenol eventually produces organic acids such as oxalic, maleic, and formic acid, which account for the subsequent drop in pH. Eventually, these daughter acids are further degraded at the anode surface by surface-bound hydroxyl radicals to aqueous CO_2 (e.g., $\text{CO}_2 \cdot \text{H}_2\text{O}$, HCO_3^- , CO_3^{2-}) with the subsequent release of gaseous carbon dioxide that accounts for the slight increase of the pH at 38 min of electrolysis

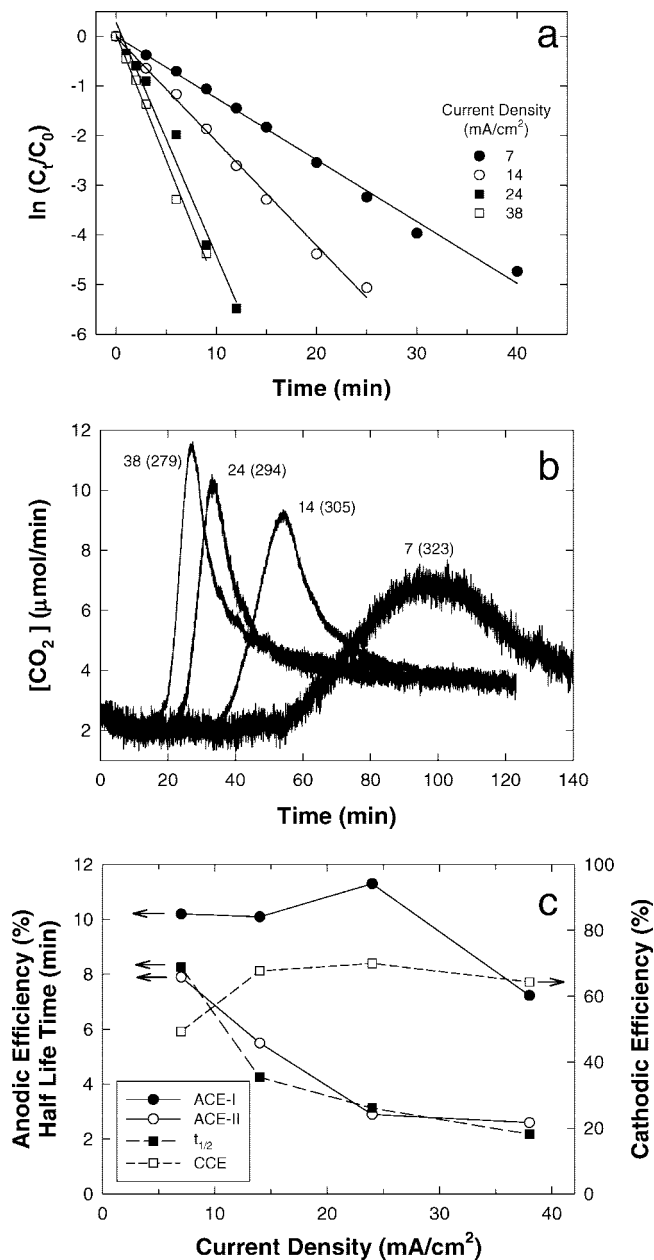


Figure 3. Effects of I_{cell} on (a) degradation of phenol, (b) release of carbon dioxide, and (c) half-life time ($t_{1/2}$) for degradation of phenol, anodic efficiencies (ACE-I, ACE-II: see Experimental Section), and cathodic efficiencies (CCE). Experimental conditions are identical to those of Figure 2.

(Scheme 3). This is the time that measurable CO_2 is initially released from the reactor (Figure 2a vs Figure 6).

At pH 10, phenol is partially deprotonated ($pK_a = 9.98$) while the BiO_x - TiO_2 anode due to the presence of Lewis acid metals (e.g., Bi) at the surface should be positively charged despite the predominance of TiO_2 (pH_{zpc} of $TiO_2 \approx 6.8$). Thus, the ability of phenol to react directly at the anode surface at pH 10 is possible, but the degree of interaction is unlikely to be strong. In contrast, substrates that are able to strongly adsorb to the anode via surface complexation should be oxidized quickly and immediately release CO_2 by multielectron transfers instead of sequential one-electron transfers. This conjecture is confirmed by the results shown in Figure 7 for the oxidation of catechol ($pK_{a1} = 9.45$; $pK_{a2} = 12.8$).³¹ Catechol functions as monodentate or bidentate ligand binding at one or two surface titanol groups. Thus, as soon as the electrolysis is initiated, CO_2 is immediately

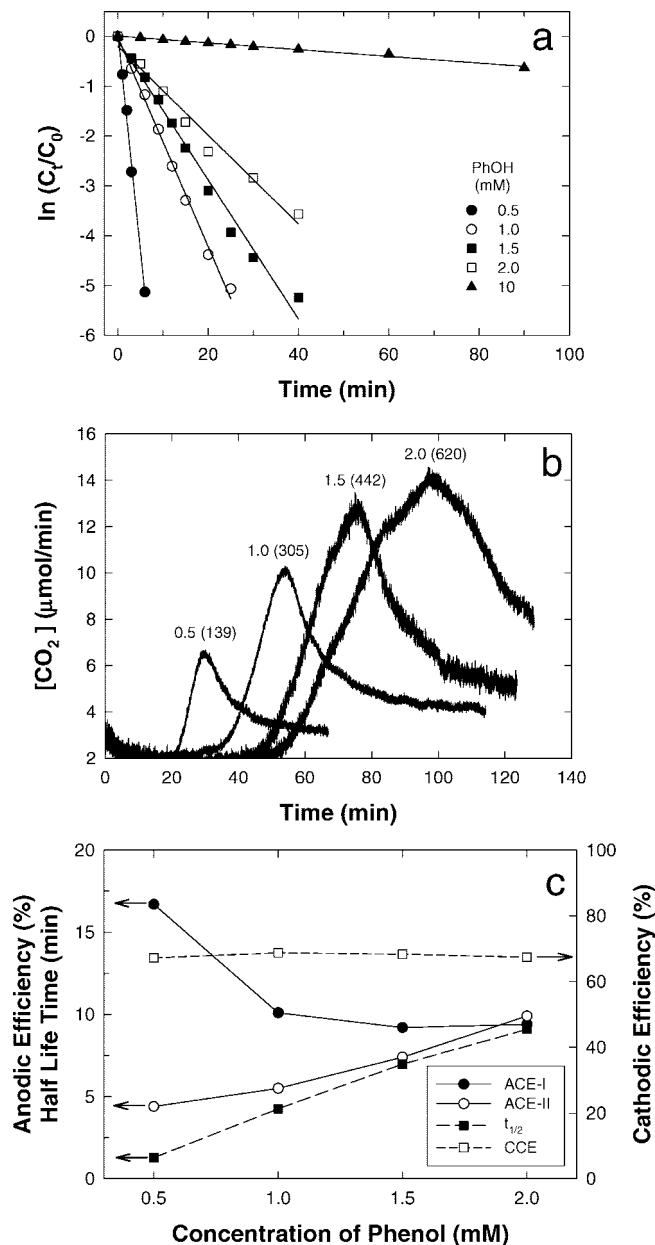


Figure 4. Effects of phenol concentration on (a) degradation of phenol, (b) release of carbon dioxide, and (c) half-life time ($t_{1/2}$) for degradation of phenol, anodic efficiencies (ACE-I, ACE-II), and cathodic efficiencies (CCE). $I_{cell} = 14$ mA/cm².

released from solution and continues over the 2 h period of electrolysis. Salicylic acid ($pK_{a1} = 2.97$; $pK_{a2} = 13.74$) also shows the same behavior. Both compounds have been known to chelate TiO_2 particle (as depicted on the right-hand side of Figure 7),^{31,32} and multiple electrons can be transferred to the anode within a few seconds after the initiation of electrolysis. Nevertheless, the first order-rate constants for disappearance of catechol and salicylic acid are lowered by approximately 50% as compared to phenol ($k_{catechol}/k_{phenol} = 0.59$; $k_{salicylic\ acid}/k_{phenol} = 0.41$). In the case of phenol, the charges are almost equally transferred to all of the phenol (and intermediates) uniformly distributed in the bulk, whereas in the cases of catechol and salicylic acid, the charges are preferentially transferred to the adsorbed molecules rather than the ones remaining in the bulk. This should result in immediate and complete oxidation of the adsorbed molecule but overall slower oxidation rate of the molecules in the bulk.

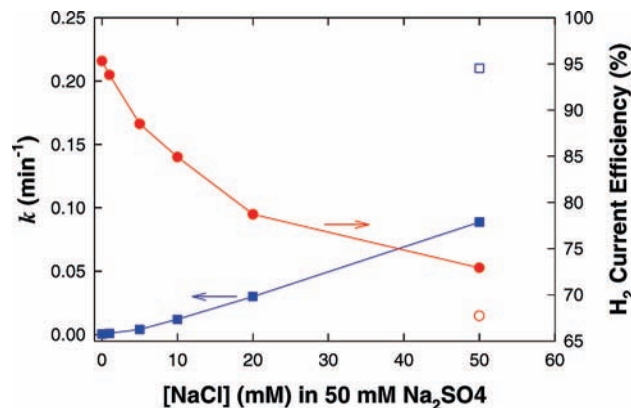


Figure 5. Effect of sodium chloride concentrations on the degradation rate (k) of phenol (■) and the current efficiency for hydrogen production (●) in 50 mM Na_2SO_4 . For comparison, effect of 50 mM NaCl without Na_2SO_4 was also shown for k (□) and hydrogen production (○). The current efficiency for hydrogen = (number of H_2 molecules \times 2)/(number of electrons) \times 100%.

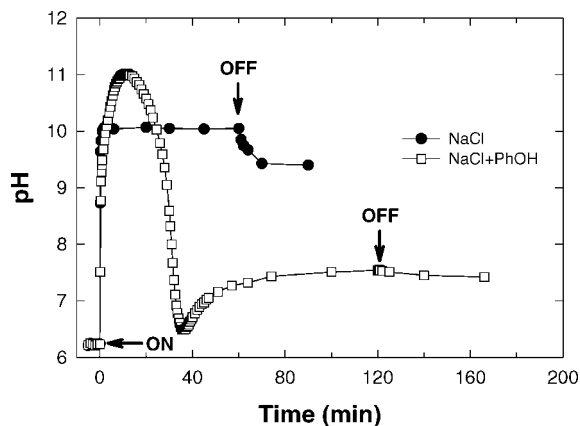


Figure 6. Time profiles of pH change during the course of electrolysis at $I_{\text{cell}} = 14 \text{ mA/cm}^2$ in the absence and presence of 1 mM phenol.

3.3. Solar Powered Electrolysis and Scale-Up. Figure 8 shows the PV-connected hybrid reactor system and reactions under different solar light irradiation conditions. The solar light radiation energy of B ($I_{\text{S,B}}$) is measured at $0.1 \pm 0.005 \text{ W/cm}^2$, while that of A ($I_{\text{S,A}}$) is around $0.107 \pm 0.005 \text{ W/cm}^2$. The overall reaction processes are similar to those in Figure 2a. As soon as the PV is connected to the electrode couples, hydrogen and oxygen are evolved, and phenol is degraded following apparent first-order kinetic along with release of carbon dioxide at the latter stage of the electrolysis. The difference of incident solar energy only affects the rate of hydrogen production; the degradation rate of phenol, the rate of oxygen generation, and the amount (i.e., the rate) of carbon dioxide released are almost invariable. At the condition B, the energy efficiency for the hydrogen production is around 30%. According to the manufacturer, a theoretical maximum power of the PV_{peak} is $6.4 \text{ W}_{\text{peak}}$ corresponding to 4.5% of the average solar light radiation energy ($I_{\text{S,0}} = 0.11 \text{ W/cm}^2$). However, when the PV is directly connected to the electrode couple, the power applied to the electrolysis (PV_{cell}) was ca. 3.5 W ($3.9 \text{ V} \times 0.9 \text{ A}$). This corresponds to 55% of the PV_{peak} and 2.5% of the $I_{\text{S,0}}$.

To investigate the effect of solar flux on the PV power and the H_2 production, the PV-connected hybrid reactor was tested on a cloudy day. As shown in Figure 9, I_{S} , E_{cell} , and I_{cell} change in the ranges of $0.1\text{--}0.08 \text{ W/cm}^2$, $4.1\text{--}3.7 \text{ V}$, and $0.7\text{--}0.9 \text{ A}$, respectively. The I_{S} continually decreases during the period of 15–50 min of electrolysis, and the PV_{cell} and the H_2 production

rate also follow the trend. However, upon addition of phenol to the reactor at 52 min, the H_2 production rate substantially increases despite the continual decrease of I_{S} and PV_{cell} . The H_2 production rate is lowered after reaching maximum range ($\sim 0.21 \text{ mmol/min}$). This behavior is observed again at subsequent phenol addition at around 80 min. This synergy effect was qualitatively explained elsewhere.¹⁸ Intermediate reactive species (HO^\cdot , Cl^\cdot , $\text{Cl}_2^{\cdot-}$, HClO/ClO^-) produced at the anode play a role of an electron shuttle and are reduced at the cathode. This reduction is thermodynamically favored over proton/water reduction. However, as the added organic compounds react with the radical species, more cathodic electrons are available for proton/water reduction, thereby increasing H_2 production energy efficiencies by as much as 30–53% at low I_{cell} .

The PV_{cell} is correlated with the I_{S} without and with phenol addition (Figure 10a). Without phenol addition (i.e., pure electrolysis), the PV_{cell} efficiency ($=\text{PV}_{\text{cell}}/I_{\text{S}} \times 100\%$) is determined to be 2.0–2.8%. A lower efficiency than the supplier-reported one ($\text{PV}_{\text{peak}} = 4.5\%$) is probably due to overestimation of the array performance by the supplier and a conversion efficiency loss by the heating of the array and ohmic drop at the reactor.³³ Nevertheless, the PV_{cell} efficiency increases linearly by 1.5 times from average 2.37% to 3.58% simply by phenol addition. The presence of phenol molecule also affects the electrolytic H_2 energy efficiency and behavior. The increasing PV_{cell} increases the electrolytic H_2 production with an average efficiency of 22% ($=\text{H}_2 \text{ energy}/\text{PV}_{\text{cell}}$ in Figure 10b). However, in the presence of phenol, the H_2 energy has no linear correlation with the PV_{cell} ; instead, it changes according to weather conditions along with phenol and intermediate degradation kinetics. At the time of phenol addition, the electrolytic H_2 energy efficiency is around 20%; yet it reaches around 40% at a much lower PV_{cell} ($2.1 \times 10^{-3} \text{ W/cm}^2$). The overall solar-to- H_2 energy efficiencies ($=\text{H}_2 \text{ energy}/I_{\text{S}} \times 100\%$) also are similar. In the absence of phenol, the overall efficiency is on average 0.67% on the average (Figure 10c). The electrolysis of phenol increases the overall efficiency from 0.53% ($5.5 \times 10^{-4} \text{ W cm}^{-2}/1.03 \times 10^{-1} \text{ W cm}^{-2}$) to 1.0% ($8.1 \times 10^{-4} \text{ W cm}^{-2}/8.1 \times 10^{-2} \text{ W cm}^{-2}$), which is similar to the efficiency in Figure 8.

For application to pilot or subpilot scale, a batch reactor of 20 L-size was prepared where 5 anodes (each, $800 \text{ cm}^2/\text{anode}$) and 6 cathodes of the same size are arranged to alternatively face each other (Scheme 2b). At 60 W ($3 \text{ V} \times 20 \text{ A}$) of power, carbon dioxide starts being released after 20 min, and the rate of hydrogen production reaches ca. $3.5 \times 10^{-3} \text{ mol/min}$ with a hydrogen energy efficiency of 28% (Figure 11a). The half-life of 1 mM phenol in a total volume of 20 L is $<2 \text{ min}$. On the basis of this operating conditions, we can estimate the required PV areas with different efficiencies (i.e., PV_{cell} efficiency = $\text{PV}_{\text{cell}}/(I_{\text{S,0}} \times \text{PV area}) \times 100\%$) for treating variable capacity of water/wastewater contaminated with 1 mM phenol (Figure 11b). It is clear water treatment capacity is strongly related to the PV area and efficiency. For example, treatment of 16 tons of water (i.e., 1.6 kg of phenol) daily (i.e., operation for 9 h/day) needs a 62 m^2 PV panel operating at 10% efficiency. In addition, hydrogen is obtained as a potentially useful byproduct. Hydrogen production rates are affected both by the water treatment capacity and by H_2 energy efficiency (Figure 11c). Small-scale reactors are usually better than large reactors for the energy efficiency. At a H_2 energy efficiency of 60%, the treatment of 16 tons of water with a PV of 10% efficiency will yield around 1 kg of H_2 daily.

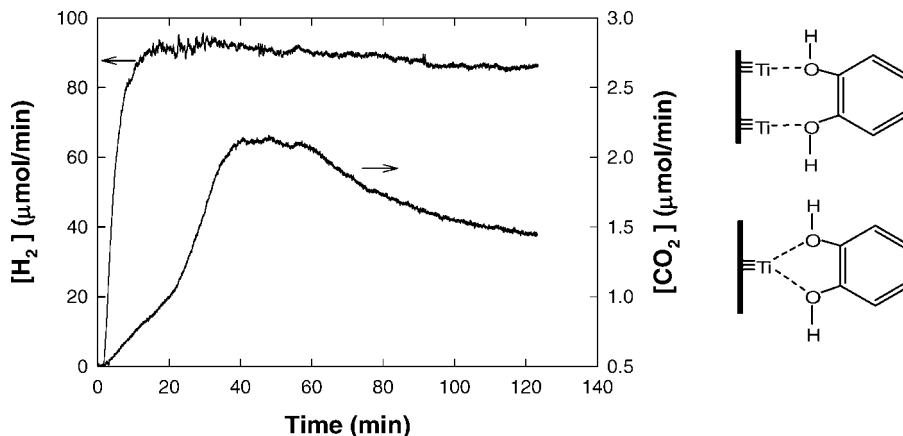


Figure 7. Simultaneous production of hydrogen and carbon dioxide during the course of electrochemical oxidation of 1 mM catechol at $I_{\text{cell}} = 12.8$ mA/cm².

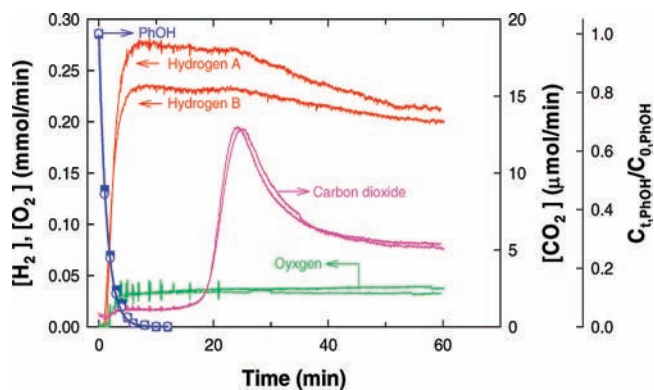


Figure 8. Solar-powered oxidation of phenol to carbon dioxide and simultaneous nonstoichiometric water splitting. A 6.4 W-rated photovoltaic cell with area of 1280 cm² is directly connected to the anode–cathode couple. Hydrogen A and B indicates the hydrogen production at solar energy of 1.00 ± 0.01 and 1.07 ± 0.01 W/cm², respectively.

3.4. Technical Consideration. Electrodes. Electrolytic water splitting typically employs Pt group metals (PGM) as anodes and Ni-based alloy (e.g., Ni–Zn, Ni–Al, Ni–Co, Ni–Mo–Cd),^{34–36} stainless steel,³⁶ or noble metals (e.g., Pt, Au) as cathodes and operates at extreme conditions such as high concentration of electrolyte (> 1.0 mol/L), high pH (> 1.0 mol/L KOH), and high pressure. The main reason for employing the Pt-based anode is that Pt efficiently enables catalytic four-electron oxidation of water (R3). However, for the electrochemical oxidation of organic compounds (R4), the anode should generate preferentially radical species (e.g., HO[•], Cl[•]), which are either surface-bound or mobile ones.

A variety of anodes such as single metal oxides (e.g., PbO₂,^{24,25,37–41} SnO₂,^{24,37,39,42} IrO₂,^{42,43} RuO₂,⁴³), multiple metal oxides (e.g., Ta₂O₅/IrO₂,⁴⁴ Bi–PbO₂/Pt,⁴⁰ PbO₂/SnO₂,⁴⁵ IrO₂/RuO₂/TiO₂,⁴⁶), and boron-doped diamond (BDD)⁴⁷ have been developed for the treatment of aqueous chemicals. For example, PbO₂ coated on titanium substrate has been widely studied; however, a possibility of release of lead ions anode stability concerns are a serious drawback to practical application. BDD electrode also has been greatly paid attention to due to its stability and wide potential window;⁴⁷ yet the extremely high price makes it impossible for application at the pilot scale. Pt could be applied to wastewater treatment. However, it is known to be readily deactivated in case of oxidation of phenol due to formation of a polymeric film on its surface, leading to lower efficiency.^{22,48,49} On the other hand, the BiO_x–TiO₂ anode

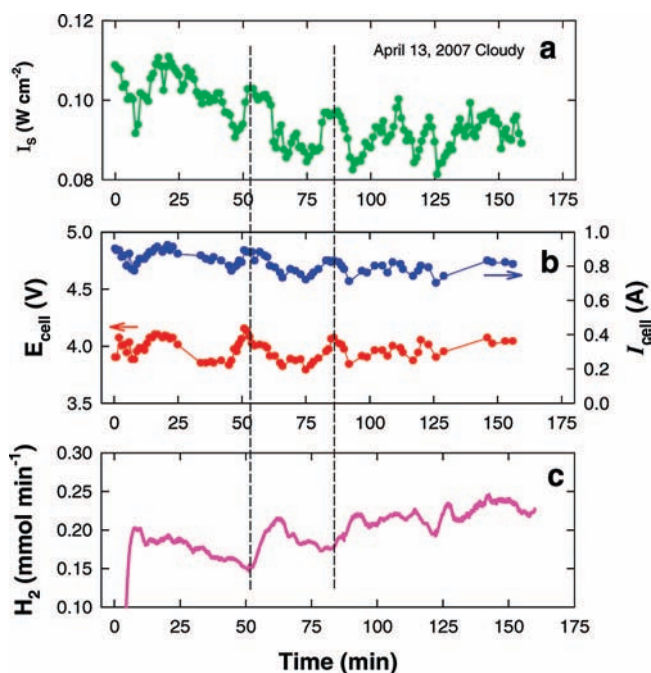


Figure 9. Real-time profiles of solar powered electrolysis without and with phenol addition on a cloudy day (April 13th, 2007). A 6.4 W-rated photovoltaic cell with area of 1280 cm² is directly connected to the anode–cathode couple. I_s , solar light radiation energy (W/cm²); E_{cell} , cell voltage (V); I_{cell} , cell current (A). 1 mM phenol was successively added at 52 and 87 min of electrolysis as indicated by dotted lines.

employed in this study is found to be very stable and show good current yield in the range of 25–36% for oxidation of propylene glycol.¹⁷ In addition, it has been manufactured at the subpilot scale in the size range of square meter with relatively low costs. Also, various types of cathodes are available. However, in the practical point of the water treatment in the sub- or pilot scale, SS is the most feasible in cost, stability, and availability. Surface treatment of SS (e.g., Ni or Pt-coating) could improve the efficiency of electron transfer.^{50,51}

Technical Comparison. It should be noted that this PV–electrolysis–water treatment system is different from the conventional PV–electrolyzer as follows. First, few experimental studies on combined PV–electrolyzer technologies operating at mild conditions have actually been reported. For example, Ahmad and Shenway examined a PV-driven electrolysis system for hydrogen production with reported electrolysis efficiencies of 60% in a 27% KOH solution (~ 4.8 mol/L; pH 14.7).⁶ Comparison of the solar-to-H₂ energy efficiency

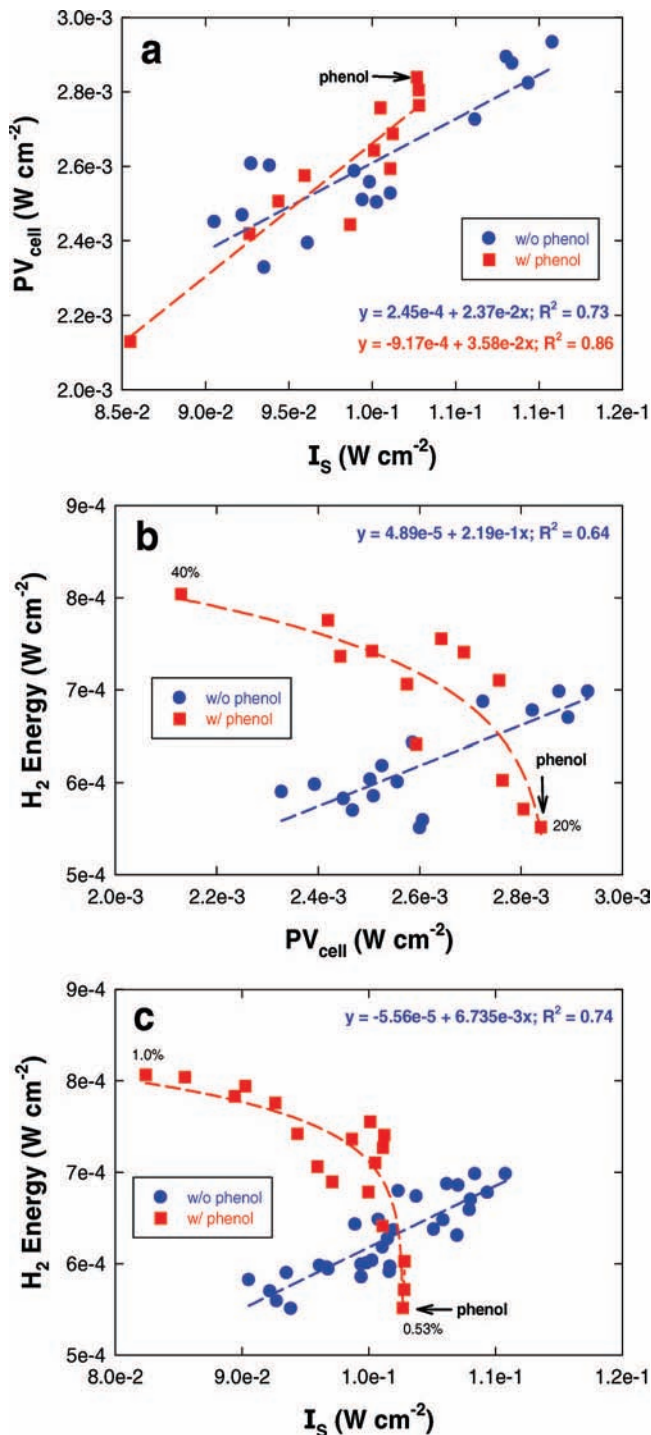


Figure 10. Relationships of (a) I_s vs PV_{cell} , (b) PV_{cell} vs H_2 energy, and (c) I_s vs H_2 energy without and with phenol addition during electrolysis.

is not reliable due to different purpose and conditions (Table 1). A high-powered and -efficient PV usually has a high solar-to- H_2 efficiency. Photovoltaic arrays of 5–9 kW PV_{peak} and 8.1–8.4% PV_{cell} efficiency coupled with alkaline electrolyzer (30% KOH) of 62–77% electrolytic H_2 efficiency have overall solar-to- H_2 efficiency of 3.6–6.2%.^{33,52} The alkaline electrolyzer of similar electrolytic H_2 efficiency (60%) has a much lower solar-to- H_2 efficiency of 1.5% when coupled to a low-powered PV_{peak} (53 W).⁶ Because of the extremely high electrolyte concentration, which is a general condition for maximizing the efficiency in the alkaline electrolysis, their system as well as other electrolysis systems are practically impossible to apply

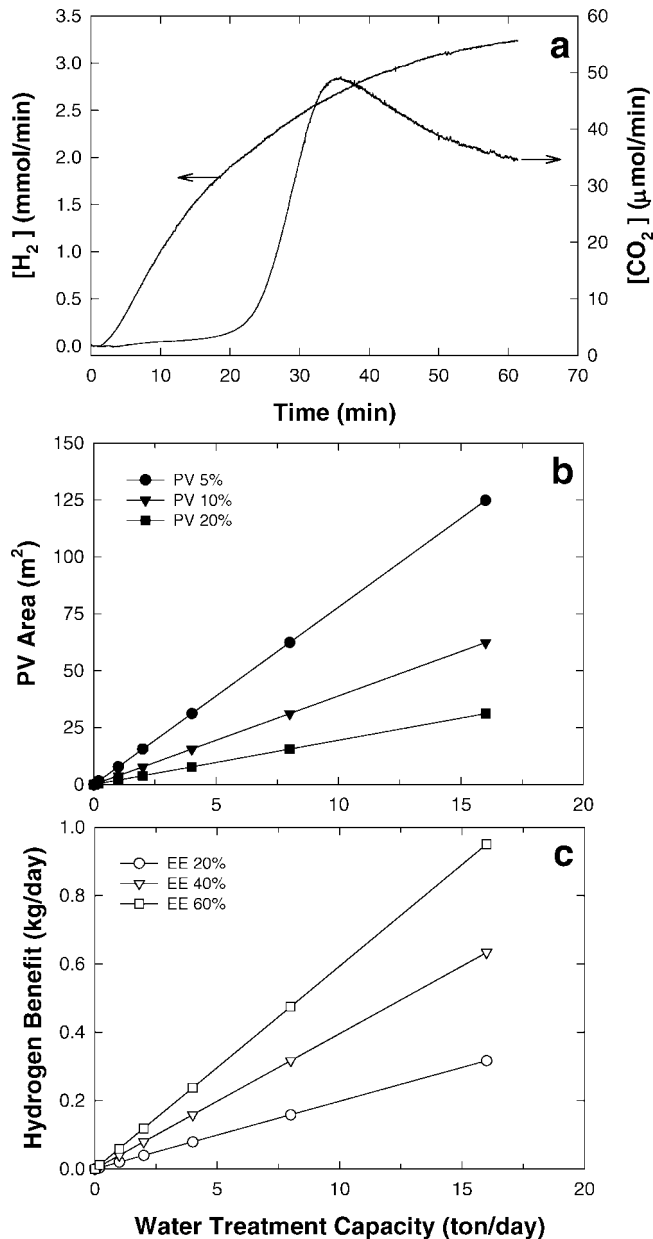


Figure 11. (a) A DC-powered electrochemical oxidation of phenol to carbon dioxide and generation of hydrogen in a subpilot scaled reactor (20 L) at $E_{cell} = 3$ V and $I_{cell} = 20$ A. $[phenol]_0 = 1$ mM. (b) Correlation between water treatment capacity and required PV area with different efficiencies. (c) Effects of water treatment capacity on the amount of hydrogen obtainable with different energy efficiencies at a PV_{cell} of 10%. (b) and (c) were estimated on the basis of the operation of the subpilot scaled reactor. Capacity of water treatment = 20 L/h (1 mM phenol) at 60 W (3 V \times 20 A); daily solar utilization time (working hours) = 9 h (9 am to 6 pm, California); average solar energy input = $1100\ W/m^2$; PV_{cell} (PV%) = $1100\ W/m^2 \times PV_{peak} \times$ application factor (0.7).

to large scale water purification and treatment. In comparison, our system operates over similar efficiency (electrolytic H_2 energy efficiency $>30\%$; solar-to- H_2 energy efficiency $\sim 1.0\%$) with a low-powered PV_{peak} (6.4 W) at 2 orders of magnitude lower electrolyte concentration ranges (2×10^{-2} to 5×10^{-2} mol/L).

Second, PV–electrolyzer systems on a laboratory or pilot scale have been considered and examined as alternatives to a system of PV–electricity–battery. The systems are typically and primarily composed of PV arrays for converting solar light

TABLE 1: Comparison of PV–Electrolysis Energy Efficiencies (EEs)

PV _{peak}	electrode	electrolyte	purpose	average solar-to-PV EE ^a	average electrolytic H ₂ EE ^b	average solar-to-H ₂ EE ^c	ref
5 kW _p		30 wt % KOH	H ₂ storage and fuel cell	8.4%	62%	3.6%	33
53 W _p	Ni/Ni	27 wt % KOH	H ₂ storage and fuel cell		60%	1.5%	6
9.2 kW _p	bipolar alkaline electrolyzer	bipolar alkaline electrolyzer	H ₂ storage and fuel cell	8.1%	77%	6.2%	52
6.4 W _p	BiO _x –TiO ₂ /SS	0.27 wt % NaCl	hybrid	2.5%	30–60%	1.0%	this study

^a PV_{cell}/I_s. ^b H₂ energy/PV_{cell}. ^c H₂ energy/I_s.

to electricity, alkaline electrolyzers for producing hydrogen using the electricity, hydrogen storage tanks, and fuel cells for producing electricity from the stored hydrogen (and oxygen). Therefore, the primary goal of these studies is to utilize hydrogen as a storable medium for the dark generation of electricity. However, the PV–electrolyzer systems, which produce hydrogen, are found to be economically impractical as compared to conventional PV–electricity–battery combinations. For example, total annual cost and net cost of the electricity of the former are around 3 and 4 times higher than those of the latter, respectively.⁸ The hydrogen produced from a typical PV–electrolyzer system is substantially more expensive than the SMR. On the other hand, if the hydrogen production can be combined with water and wastewater treatment, then PV–electrolyzer systems are economically viable.^{53,54}

This hybrid system should be distinguished from reported electrochemical hybrid systems for hydrogen production and chemical oxidation in terms of practical operation and efficiency. Most hybrid systems operate with limited number of organic chemicals and low efficiency. For example, a DC-powered electrolytic hydrogen production from organic chemicals in water was reported, but the system works only for methanol (i.e., a reversed direct methanol fuel cell process).¹² A hybrid system of electro-assisted photo-Fenton oxidation and cathodic hydrogen production was described; yet the system operates only for a limited number of substrates at very limited conditions and needs post-treatments like separation of the reagents.¹⁰ In contrast, our system has been proven to decompose and mineralize a variety of phenolic compounds (e.g., phenol, mono-, di-, trichlorinated phenols, catechol, hydroquinone, resorcinol, salicylic acids, etc.), aliphatic acids (e.g., maleic acid, malonic acid, oxalic acid, fumaric acid, polypropylene, etc.), and dyestuffs (methyl orange, *ortho*-methyl red, *para*-methyl red, methylene blue, acid orange 7, rhodamine B, etc.).^{18,19} These chemicals are commonly found in industrial and domestic wastewaters.

Application. Some problems would limit application of the hybrid system to the conventional water treatment facility. First is the electrolyte (i.e., NaCl), which is intrinsically necessary for the electrolysis. However, the sodium chloride is the most abundant constituent of water/wastewater stream in the range 1–9300 kg/day,²¹ and wastewater inflows have a high conductivity in the range of 620–3550 μS/cm.⁵⁵ In addition, this hybrid is found to work efficiently even at 21 mM NaCl (~1.2 g/L).¹⁷ The other is that the electrolysis could produce some toxic byproducts. However, no chlorinated gases such as methyl chloride, dichloromethane, chloroform, tetrachloride, phosgene, vinyl chloride, and chlorine were detected during the electrolysis in the presence of phenol. The chlorinated phenols, which are produced, are very rapidly converted to carbon dioxide (e.g., $k_{2,4,6\text{-ClPhOH}}/k_{\text{PhOH}} > 3.7$), water, and chloride.

Separation and purification of the evolved gas stream is absolutely necessary. However, it is not a difficult challenge. Proton-exchange membranes such as Nafion or porous ceramic

separators (e.g., fine glass frit) can be put between the anode and cathode. Because oxygen and carbon dioxide are produced at the anode, both gases are effectively separated from hydrogen produced at the cathode provided that there is an appropriate membrane separating the two compartments. In addition, even if hydrogen is mixed with carbon dioxide, CO₂ can be readily removed just by chemical absorption process (e.g., flowing carbon dioxide gas through amine solution), which is a typical CO₂ separation process in gas turbine power plants.

Current water and wastewater treatment processes include a pretreatment for steps to screen out solid debris and large particle suspended solids, physical separation such as small particle coagulation, flocculation and sedimentation, flotation and clarification, biological treatment for removal of microbial oxygen demand, and advanced oxidation treatment such as UV/ozone process for disinfection and reduction of chemical oxygen demand. Therefore, no unit process itself could replace the overall wastewater treatment processes. Our PV–electrolytic system would replace conventional UV/ozone steps as an advanced oxidation and disinfection alternative.

Acknowledgment. Research was supported by the Daegu Gyeongbuk Institute of Science and Technology (DGIST), the KOSEF Nano R&D program (Grant No. 2005-02234), and the Hydrogen Energy Research & Development Center and 21st Century Frontier Research and Development Program of the Ministry of Science and Technology of Korea.

References and Notes

- (1) International Energy Outlook 2006, Energy Information Administration.
- (2) Penner, S. S. *Energy* **1998**, *23*, 71.
- (3) Hydrogen Market, Hydrogen R&D and Commercial Implication in the U.S. and E.U., available at: <http://www.researchandmarkets.com/reports/301714>, 2005.
- (4) Solar and Wind Technologies for Hydrogen Production, available at: http://www.hydrogen.energy.gov/congress_reports.html.
- (5) Korposki, B.; Levene, J.; Harrison, K.; Sen, P. K.; Novachek, F. *Electrolysis: Information and Opportunities for Electric Power Plants*, available at: <http://www.osti.gov/bridge>.
- (6) Ahmad, G. E.; El Shenawy, E. T. *Renewable Energy* **2006**, *31*, 1043.
- (7) Turner, J. A. *Science* **1999**, *285*, 687.
- (8) Friberg, R. *Int. J. Hydrogen Energy* **1993**, *18*, 853.
- (9) Szyszka, A. *Int. J. Hydrogen Energy* **1998**, *23*, 849.
- (10) Soler, L.; Macanas, J.; Munoz, M.; Casado, J. *Int. J. Hydrogen Energy* **2006**, *31*, 129.
- (11) Mathieson, G.; Langdon, A.; Jamieson, G. *Dev. Chem. Eng. Miner. Process.* **2006**, *14*, 71.
- (12) Narayanan, S. R.; W., C.; Jeffries-Nakamura, B.; Valdez, T. I. *Hydrogen Generation by Electrolysis of Aqueous Organic Solutions*. U.S. Patent 6,368,492, April 9, 2002.
- (13) Kesselman, J. M.; Weres, O.; Lewis, N. S.; Hoffmann, M. R. *J. Phys. Chem. B* **1997**, *101*, 2637.
- (14) Weres, O.; Hoffmann, M. R. *Electrode, Electrode Manufacturing Process and Electrochemical Cell*. U.S. Patent 5,419,824.
- (15) Weres, O.; Hoffmann, M. R. *Electrochemical Method and Device for Generating Hydroxyl Free Radicals and Oxidizing Chemical Substances Dissolved in Water*. U.S. Patent 5,364,508, Nov. 15, 1994.

- (16) Weres, O.; Hoffmann, M. R. Electrochemical Device for Generating Hydroxyl Free Radicals and Oxidizing Chemical Substances Dissolved in Water. U.S. Patent 5,439,577, Aug. 8, 1995.
- (17) Weres, O. Electrode with Surface Comprising Oxides of Titanium and Bismuth and Water Purification Process Using This Electrode. U.S. Patent 0,000,774 A1, Jan. 4, 2007.
- (18) Park, H.; Vecitis, C. D.; Choi, W.; Weres, O.; Hoffmann, M. R. *J. Phys. Chem. C* **2008**, *112*, 885–889.
- (19) Park, H.; Vecitis, C. D.; Hoffmann, M. R. *J. Phys. Chem. C* **2008**, submitted.
- (20) Glassmeyer, S. T.; Furlong, E. T.; Kolpin, D. W.; Cahill, J. D.; Zaugg, S. D.; Werner, S. L.; Meyer, M. T.; Kryak, D. D. *Environ. Sci. Technol.* **2005**, *39*, 5157.
- (21) Barber, L. B.; Murphy, S. F.; Verplanck, P. L.; Sandstrom, M. W.; Taylor, H. E.; Furlong, E. T. *Environ. Sci. Technol.* **2006**, *40*, 475.
- (22) Gattrell, M.; Kirk, D. W. *J. Electrochem. Soc.* **1993**, *140*, 903.
- (23) Canizares, P.; Martinez, F.; Diaz, M.; Garcia-Gomez, J.; Rodrigo, M. A. *J. Electrochem. Soc.* **2002**, *149*, D118.
- (24) Kotz, R.; Stucki, S.; Carcer, B. *J. Appl. Electrochem.* **1991**, *21*, 14.
- (25) Tahar, N. B.; Savall, A. *J. Electrochem. Soc.* **1998**, *145*, 3427.
- (26) Boudenne, J. L.; Cerclier, O.; Bianco, P. *J. Electrochem. Soc.* **1998**, *145*, 2763.
- (27) Korbahiti, B. K.; Salih, B.; Tanyolac, A. *J. Chem. Technol. Biotechnol.* **2002**, *77*, 70.
- (28) Buxton, G. V.; Greenstock, C. L.; Helman, W. P.; Ross, A. B. *J. Phys. Chem. Ref. Data* **1988**, *17*, 513.
- (29) Hasegawa, K.; Neta, P. *J. Phys. Chem.* **1978**, *82*, 854.
- (30) Gallard, H.; von Gunten, U. *Environ. Sci. Technol.* **2002**, *36*, 884.
- (31) Araujo, P. Z.; Morando, P. J.; Blesa, M. A. *Langmuir* **2005**, *21*, 3470.
- (32) Tunesi, S.; Anderson, M. *J. Phys. Chem.* **1991**, *95*, 3399.
- (33) Hollmuller, P.; Joubert, J. M.; Lachal, B.; Yvon, K. *Int. J. Hydrogen Energy* **2000**, *25*, 97.
- (34) Los, P.; Rami, A.; Lasia, A. *J. Appl. Electrochem.* **1993**, *23*, 135.
- (35) Navarro-Flores, E.; Chong, Z. W.; Omanovic, S. *J. Mol. Catal. A* **2005**, *226*, 179.
- (36) Radhakrishnamurthy, P.; Sathyanarayana, S.; Reddy, A. K. N. *J. Appl. Electrochem.* **1977**, *7*, 51.
- (37) Rodgers, J. D.; Jedral, W.; Bunce, N. I. *Environ. Sci. Technol.* **1999**, *33*, 1453.
- (38) Bonfatti, F.; Ferro, S.; Lavezzo, F.; Malacarne, M.; Lodi, G.; De Battisti, A. *J. Electrochem. Soc.* **2000**, *147*, 592.
- (39) Bonfatti, F.; Ferro, S.; Lavezzo, F.; Malacarne, M.; Lodi, G.; De Battisti, A. *J. Electrochem. Soc.* **2000**, *147*, 592.
- (40) Iniesta, J.; Exposito, E.; Gonzalez-Garcia, J.; Montiel, V.; Aldaz, A. *J. Electrochem. Soc.* **2002**, *149*, D57.
- (41) Kaba, L.; Hitchens, G. D.; Bockris, J. O. *J. Electrochem. Soc.* **1990**, *137*, 1341.
- (42) Comninellis, C.; Nerini, A. *J. Appl. Electrochem.* **1995**, *25*, 23.
- (43) Kim, K. W.; Lee, E. H.; Kim, J. S.; Shin, K. H.; Jung, B. I. *J. Electrochem. Soc.* **2002**, *149*, D187.
- (44) Fino, D.; Jara, C.; Saracco, G.; Specchia, V.; Spinelli, P. *J. Appl. Electrochem.* **2005**, *35*, 405.
- (45) Gherardini, L.; Michaud, P. A.; Panizza, M.; Comninellis, C.; Vatas, N. *J. Electrochem. Soc.* **2001**, *148*, D78.
- (46) Rajkumar, D.; Kim, J. G.; Palanivelu, K. *Chem. Eng. Technol.* **2005**, *28*, 98.
- (47) Panizza, M.; Cerisola, G. *Electrochim. Acta* **2005**, *51*, 191.
- (48) Koile, R. C.; Johnson, D. C. *Anal. Chem.* **1979**, *51*, 741.
- (49) Boudenne, J. L.; Cerclier, O.; Galea, J.; VanderVlist, E. *Appl. Catal., A* **1996**, *143*, 185.
- (50) Whalen, J. J.; Weiland, J. D.; Searson, P. C. *J. Electrochem. Soc.* **2005**, *152*, C738.
- (51) Dominey, R. N.; Lewis, N. S.; Bruce, J. A.; Bookbinder, D. C.; Wrighton, M. S. *J. Am. Chem. Soc.* **1982**, *104*, 467.
- (52) Lehman, P. A.; Chamberlin, C. E.; Pauletto, G.; Rocheleau, M. A. *Int. J. Hydrogen Energy* **1997**, *22*, 465.
- (53) Phenolic Wastewater Treatment Alternatives, Air Force Engineering and Service Center Tyndall AFB FL Engineering and Services Lab, Air Force Engineering and Services Center, 1980.
- (54) Jones, O. A. H.; Green, P. G.; Voulvoulis, N.; Lester, J. N. *Environ. Sci. Technol.* **2007**, *41*, 5085.
- (55) Conn, K. E.; Barber, L. B.; Brown, G. K.; Siegrist, R. L. *Environ. Sci. Technol.* **2006**, *40*, 7358.

JP802807E